Progress In Electromagnetics Research M, Vol. 31, 231–246, 2013

REALIZATION OF LINEAR-TO-CIRCULAR POLARIZATION CONVERSION BY A SINGLE BIFILAR PARTICLE

Alexei Balmakou[1, 2, *], Igor Semchenko[2], and Masaaki Nagatsu[1]

[1]Department of Nanovision Technology, Graduate School of Science and Technology, Shizuoka University, Hamamatsu, Japan

[2]Department of Physics, Gomel State University, Gomel, Belarus

Abstract—In this paper, we provide a new theoretical model describing mechanism of electromagnetic radiation (and scattering) by passive single- and double-stranded (bifilar) helices. The proposed model is derived from basic physical principles till the end formulas which were computer processed for predicting a polarization type of the wave scattered by a helix. Comparison of the two types of helical oscillators revealed radical differences in their scattering performance (intensity and polarization). Optimal parameters of the bifilar helix for transformation of the polarization state from linear to circular were found for a *non-axial* direction of the incident and scattered field. Key features of the proposed model were confirmed by computer simulations.

1. INTRODUCTION

Metallic helices, which have been studied at least since 1920 [1], interest scientists today from a point of view of photonic crystal, metamaterial applications, as well as new broadband microwave and optical devices. Recent years, helix type metamaterials have been studied analytically, experimentally, and numerically [2–7] for realization of a circular polarizer based on the helix-axis wave propagation. However, the case of non-axial wave propagation is also of high interest, because it can lead to very diverse effects, e.g., it was shown that arrays composed of metal helices with some specific spatial arrangements can lead to observation of metamaterial effects such as a strong changeable electric or magnetic response [8], negative permittivity and negative

Received 9 May 2013, Accepted 6 July 2013, Scheduled 8 July 2013

* Corresponding author: Alexei Balmakou (balmakou@gmail.com).

permeability [9], circular polarization filtering [4, 10], cloaking [11], polarization rotation and transformation [12, 13], photonic stop gaps [14] and others.

In this paper, we propose a new design of a double helical particle (as a meta-atom) with the optimal shape for realization of linear-to-circular polarization conversion. The optimal shape denotes that the double stranded helix has a particular pitch angle at witch a strong scattering of circularly polarized waves towards a perpendicular to helix axis direction takes place. We have calculated this pitch angle by considering in detail an electromagnetic response in every elementary resonant fragment of the double helix and then recreated the full scattering field formed by all resonant fragments. Importantly, the incident linear wave should propagate perpendicular to the helix axis and the plane of the E-vector oscillation should cross the ends of the helix. This theoretical approach distinguishes this work from a number of related ones. In the next sections we confirm the analytical predictions by computer modeling. We emphasize the importance of the double stranded configuration of the particle, however, if the narrow directivity of the scattering is not necessary, an additional pairs of helices can be added into the particle design for more omnidirectional scattering.

2. HELICAL PARTICLE EXCITATION

Let us first theoretically consider a phenomenon of strong polarization-sensitive excitation of helices by comparing two helical particles having the same shape. The first one in Figure 1(a) represents a common single stranded (ss-) helix, while the second one in Figure 1(b) has a double stranded (ds-) structure. This simple combination of two helices into one unit radically changes its electromagnetic properties. The center of the particle is located in the origin and it can contain an integer number of half-pitches (or half-turns).

Excitation of a helix as a passive element can be realized by an external electromagnetic wave for different directions of wave propagation, but here we emphasize a non-axial incidence which leads to some promising results of practical realization. Consider, for simplicity, a linearly polarized incident plane wave impinging the helix perpendicular to its axis. In the case of the fundamental frequency resonance, when the wavelength is equal to the helix period (the length of one pitch) $\lambda = P$ and the helix diameter is small with respect to the wavelength $d < \lambda/\pi$, the helix has a specific electric current mode. Electric charges oscillate synchronously along the helix yielding the induced electric current distributed periodically

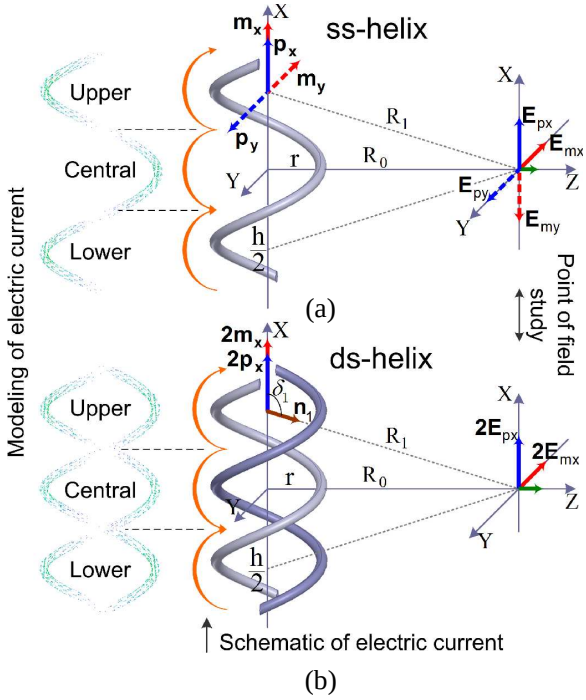

Figure 1. (a) Schematic of a ss- and (b) ds-helix where electric **p** and magnetic **m** responses are shown for the upper half-turn(s) as well as the E-field induced by them at some point in space where the field is investigated. Snapshot of the main mode of the surface electric current distribution in the particle is shown on the left (computer simulation).

with the period P. Thus, a standing wave of the electric current takes place [computer modeling snapshots are shown in Figure 1(a) for ss- and (b) for ds-helices of 3 half-turns]. The current density is represented schematically by yellow arrows with their thicknesses proportional to the current density value. In this regime, the helix re-radiates (scatters) in the so-called normal mode, which yields radiation broadside to the helix axis [15].

In general, however, the electric current in the helix may have a complex form described by the general Fourier expansion formula:

$$I(l) = \sum_{n=1}^{\infty} b_n \cos\left(n\frac{2\pi}{P}l\right), \tag{1}$$

where P is the helix period, n is an integer, l is the coordinate measured along the helix, and b_n are the coefficients of the Fourier series (they

define the amplitudes of the electric current harmonics). For $n = 1$ (the first harmonic), we get from (1) the current distribution depicted in Figure 1 ($b_n = 1$ for simplicity). It is a very strong (and easily excited) current mode resonance. The resonant electric current modes depend on the excitation wavelength, therefore, one can expect the excitation of different modes when shifting from the main resonance.

The helices, as chiral elements, are characterized by dielectric, magnetic, and chiral polarizabilities in the field of monochromatic electromagnetic waves. Therefore, the particles can be described by the following coupling equations:

$$\mathbf{p} = \varepsilon_0 \alpha_{ee} \mathbf{E} - i\sqrt{\varepsilon_0 \mu_0}\, \alpha_{em} \mathbf{H}, \quad \mathbf{m} = \alpha_{mm} \mathbf{H} + i\sqrt{\varepsilon_0 / \mu_0}\, \alpha_{me} \mathbf{E}, \qquad (2)$$

where α_{ee} and α_{mm} are the tensors of dielectric and magnetic polarizabilities; α_{em} and α_{me} are the pseudotensors characterizing the chiral properties of the helix; ε_0 and μ_0 are the electric and magnetic constants, respectively. The Onsager-Casimir principle of symmetry of kinetic coefficients yields the relationship $\alpha_{em} = \alpha_{me}^T$ [16], where T denotes the tensor transposition. Both the electric and magnetic moments (2) refer to the same elementary segment of the helix with a certain current distribution (they are determined by the shape and size of this segment).

The electric and magnetic moments induced in the every elementary segment (a half-turn in the case of Figure 1) of the helix can be read according to their definitions as:

$$\mathbf{p} = -\int\limits_{(V)} e\eta \mathbf{S}(l) dV, \quad \mathbf{m} = \frac{1}{2} \int\limits_{(V)} (\mathbf{r} \times \mathbf{j}) dV, \qquad (3)$$

where e is the electron charge, η is the volume density of electrons, $\mathbf{S}(l)$ is the electron oscillation displacement vector, $dV = S_\perp dl$ is the volume of an elementary helix segment, $S_\perp$ is the cross-sectional area of the segment, $\mathbf{r}$ is the radius-vector of the helix, $\mathbf{j}$ is the current density vector, and the cross $\times$ signifies the vector product.

The components of vectors (3) were calculated taking into account the definition of the specific torsion of the helix $|q| = 2\pi/h$, which is positive $q > 0$ for the right- and negative $q < 0$ for the left-handed helix, where h is the helix pitch:

$$\begin{Bmatrix} p_x \\ p_y \\ p_z \end{Bmatrix} = \frac{i}{\omega} qr \int\limits_{x_1}^{x_2} I(x) \begin{Bmatrix} \frac{1}{qr} \\ -\cos(qx) \\ -\sin(qx) \end{Bmatrix} dx,$$
$$\begin{Bmatrix} m_x \\ m_y \\ m_z \end{Bmatrix} = \frac{1}{2} r \int\limits_{x_1}^{x_2} I(x) \begin{Bmatrix} qr \\ xq\sin(qx) + \cos(qx) \\ \sin(qx) - xq\cos(qx) \end{Bmatrix} dx. \qquad (4)$$

Let us compare the results for the components p_x and m_x which play the dominant role in the radiation of the electromagnetic field in a direction orthogonal to the helix axis. By eliminating the current from p_x, m_x in Eqs. (4), one can find the relation

$$p_x = \frac{2i}{\omega r^2 q} m_x, \tag{5}$$

which holds valid for any current $I(x)$ mode. When retrieving components along the y- and z-axes, we assume that the current $I(x)$ satisfies the principal resonance excitation relation $n = 1$ in Eq. (1). Thus, it follows that the current is some even function. Therefore, by simple comparing y-components in Eqs. (4), we find the following approximate (as the first integral in m_y does not equal to zero) relation:

$$p_y \approx -\frac{2iq}{\omega} m_y, \tag{6}$$

and, finally, by comparing z-components of Eqs. (4), we find that $p_z = m_z = 0$.

Thus, for the ss-helix [see Figure 1(a)], equivalent electric **p** and magnetic **m** dipoles are directed along the x- and y-axis, respectively. For the ds-helix [see Figure 1(b)], however, the x-components are doubled, the y-components of the complementary half-turns have the opposite directions and, therefore, they compensate each other.

3. THEORY OF SINGLE-PARTICLE SCATTERING

Here we show how using the bianisotropic media composed of ds-helices one can realize a reflection based polarization transformer, which transforms linearly polarized incident waves into circularly polarized ones. For this, we need to find out what shape of the helix is optimal for re-radiation of circularly polarized waves in the perpendicular-to-helix-axis direction (e.g., $\pm z$-axis in Figure 1), if the linearly polarized incident wave enters the helix perpendicular to its axis (e.g., propagates along the $\pm y$-axis).

The discrete dipole radiation model is applied [17, 18], which allows us to calculate the instantaneous E-field gained from an individual half-turn(s). For segment(s) with a number k [in Figures 1(a), (b) it is exemplified for $k = 1$ (upper)], it can be done using the following formulas [19]:

$$\mathbf{E}_p = \frac{\mu_0}{4\pi R_0} \left(\ddot{\mathbf{p}}_k \times \mathbf{n}_k\right) \times \mathbf{n}_k, \quad \mathbf{E}_m = \frac{\mu_0}{4\pi c R_0} \mathbf{n}_k \times \ddot{\mathbf{m}}_k, \tag{7}$$

which are time and distance R_k dependent. Here $\mathbf{n}_k$ is the unit vector [see Figure 1(b) for $k = 1$], c is the speed of light, double dots denote

the 2nd time derivative. We consider a monochromatic $\exp(-i\omega t)$ incident wave, therefore, $\ddot{m} = -\omega^2 m$, $\ddot{p} = -\omega^2 p$. The resulting E-field can be calculated and the polarization of the radiated wave can be estimated by taking the sum of all field components from all half-turns. The ellipticity ε, which is of the main interest here, characterizes the polarization type of the wave and it is introduced through the reciprocal axial ratio as defined in the general case in [20]. For the ds-helix, however, the ellipticity calculation can be simplified by just having the ratio of the components (9): $\varepsilon = E_x/E_y$, as the phase difference between $\mathbf{p}$ and $\mathbf{m}$ (and therefore $\mathbf{E}_p$ and $\mathbf{E}_m$) is $\pi/2$ and $\mathbf{E}_p$ is orthogonal to $\mathbf{E}_m$.

The following expressions have been found for the components of the resultant electric field scattered by the ss-helix:

$$\begin{aligned} E_x &= aR_0 \sum_{k=-N}^{N} \exp\left(i\omega\frac{R_k}{c}\right)\left\{\frac{(-1)^{k+1}R_0}{R_k^3}p_x + \frac{1}{cR_k^2}m_y\right\}, \\ E_y &= a \sum_{k=-N}^{N} \exp\left(i\omega\frac{R_k}{c}\right)\left\{\frac{1}{R_k}p_y + \frac{(-1)^{k+1}R_0}{cR_k^2}m_x\right\}. \end{aligned} \tag{8}$$

For the ds-helix, the net components are

$$\begin{aligned} E_x &= 2aR_0^2 p_x \sum_{k=-N}^{N} \frac{(-1)^{k+1}}{R_k^3}\exp\left(i\omega\frac{R_k}{c}\right), \\ E_y &= \frac{2aR_0}{c}m_x \sum_{k=-N}^{N} \frac{(-1)^{k}}{R_k^2}\exp\left(i\omega\frac{R_k}{c}\right), \end{aligned} \tag{9}$$

where R_0 is the distance between the origin and the observation point (see Figure 1), $R_k = \sqrt{R_0^2 + (k\frac{h}{2})^2}$ the distance from the half-turn with number k to the same point, and k an integer ranging from $-N$ to N, $a = \frac{\mu_0\omega^2}{4\pi}\exp(-i\omega t)$.

We have performed the computer processing of Eqs. (8) and (9) to analyze the resultant polarization type for short and long helices taking into consideration Eqs. (5) and (6). In Figures 2(a), (b), the real part of the ellipticity $\mathrm{Re}(\varepsilon)$ vs. the number of half-turns N is shown for: (a) the ss-helix and (b) the ds-helix at some fixed distances: $R_0 = 30$, 60 or 100λ. The dotted lines here and later correspond to the near-field region ($R_0 < 2D^2/\lambda$) where the theory gives only approximate results, and the solid lines correspond to the far-field region ($R_0 \geq 2D^2/\lambda$), where the results are reliable, D is the largest dimension of the helix [15].

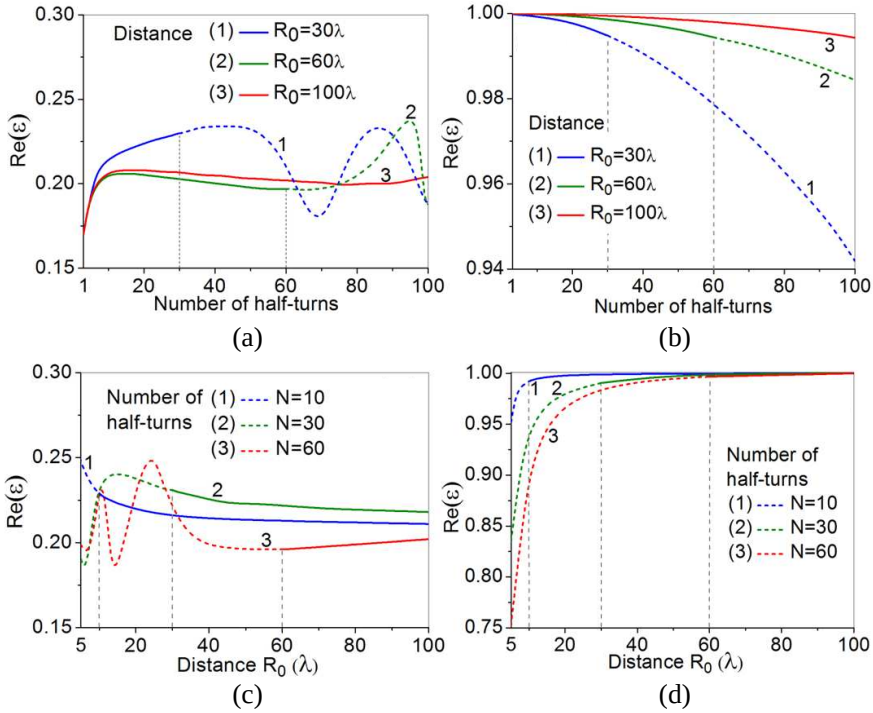

Figure 2. (a), (b) The real part of the ellipticity Re(ε) vs. the number of half-turns N; (c), (d) Re(ε) vs. the distance R_0 for: (c) the ss- and (d) ds-helix, respectively; the dashed lines correspond to the near-field region where the theory gives only approximate results, the solid lines correspond to the far-field region where the results are reliable.

From these results, one can conclude that in the far-field zone all the curves (1)–(3) give approximately the same result of near 0.17–0.24 for ss- and near unit for ds-helices. It should be noted here that the results in Figure 2 were obtained for the helices with the fixed pith angle of 24.5° [21, 22]. One can see a weak deviation of the results in the far-field region; even for a long ds-helix of 100 half-turns the ellipticity drops only less than 1% in the far-field zone. Figures 2(c), (d) show the dependence of Re(ε) on the distance R_0 for: (c) the ss- and (d) the ds-helix, when the helix is composed of $N = 10$, 30 or 60 half-turns. The correlation of the ellipticity with the corresponding graphs [(a) with (c) and (b) with (d)] is observed for the same parameters. For the ds-helices the opposite trend of curves [Figures 2(a), (b)] is observed because, with the increasing of R_0, the observation point

goes from the near-field zone towards the far-field zone, but with the increasing of N the near-field zone is expanding.

These results can be explained by means of the proposed theoretical model. With the increasing of N (and k), the angle δ_k between dipole vectors $\mathbf{p}$, $\mathbf{m}$ and the unit vector $\mathbf{n}_k$ increases too, and this leads to $\mathbf{E}_{px}$ and $\mathbf{E}_{mx}$ decreasing (the first one decreases faster), but some non-zero z-component of $\mathbf{E}$ is emerging. The last one, however, does not contribute to the wave radiated along the z-axis. On the other hand, with the increasing of R_0, the trend is the opposite, because the angle δ_k is decreasing.

For the ss-helix, however, the situation is more complicated due to the additional y-dipole-components and their opposite to $\mathbf{E}_{px}$, $\mathbf{E}_{mx}$ compensative response $\mathbf{E}_{my}$, $\mathbf{E}_{py}$. The ellipticity is determined by E_x, E_y and the phase between them [20]. Therefore, the pattern of these curves is so complex.

A helix is characterized by both its radius r and pitch h. Typically, when studying the helices, the radius and the pitch are changed independently or only the pitch itself. This approach is not convenient, because with changing only the radius (or the pitch), the resonant frequency of the particle is changing too, what is not desirable generally. Simultaneous change of the radius and the pitch can be mathematically reduced to the helix pitch angle change via:

$$\alpha = \cot^{-1}(qr). \tag{10}$$

In this case, one begins changing the helix pitch angle yielding both the radius and the pitch change, but the length of one helix pitch remains constant.

Based on the formulas for the ellipticity derived from Eq. (8) for the ss-helix and Eq. (9) for the ds-helix, it is possible to solve numerically the implicit function and explore its dependence on the pitch angle for some fixed N and R_0.

It was found that the ellipticity results to unity only for the ds-helix with $\alpha = 24.5^\circ$ (see Figure 3, curve 1). The curve has a weak dependence on N with the constant maximum position. The ss-helix exhibits the maximum ellipticity of near 0.3 at more than the doubled pitch angle in the far-field zone (see curve 2 in Figure 3). With increasing of N (or R_0), the curve 2 is deforming into the curves 3 and 4. They relate to the near-field region and, therefore, describe the ellipticity only approximately.

The same result can be derived also from the analysis of the following: Eq. (5), the relation (11) of circularly polarized wave radiation [23]:

$$|p_x| = \frac{1}{c}\,|m_x| \tag{11}$$

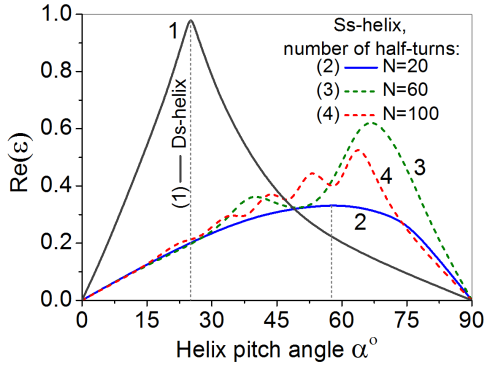

Figure 3. The real part of the ellipticity vs. the helix pitch angle for both ss- and ds-helices when $R_0 = 50\lambda$; the wave radiated by the ds-helix (curve 1) with $\alpha = 24.5°$ is circularly polarized [dependence on N for the ds-helix is negligible (no more than 5%) with the constant maximum position]; the dependence on N is shown for the ss-helix for $N = 20$ (curve 2, far-field); $N = 60$ (curve 3) and $N = 100$ (curve 4) both for the near-field zone.

as well as the main resonance condition $\lambda = P$, and the projection of the helix turn onto the yz-plane: $P\cos\alpha = 2\pi r$. Thus, the following relation is derived: $2\tan\alpha = \cos\alpha$, which yields the pith angle of circular polarization $\alpha_{CP} = 24.5°$ for the ds-helix.

Intriguingly, we can draw a parallel between the considering optimal ds-helix and B-DNA [24, 25], which is the most common form of DNA (deoxyribonucleic acid) found in nature. It has the radius $r = 1.0$–$1.3\,\text{nm}$ and the pitch $h = 3.3$–$3.4\,\text{nm}$. Thus, one can find the pitch angle range $\alpha_{\text{DNA}} = 22.0°$–$28.4°$ which contains the obtained optimal angle α_{CP}. From this point of view, the ds-helix can be called 'DNA-like', although, there is no full resemblance.

4. MODELING OF SINGLE-PARTICLE SCATTERING

Using computer simulations, we have managed to confirm the key aspects of the proposed theoretical model. Parameters of the individual helical particle (as well as periodical arrays of them) were modeled by using the commercial finite element method solver for electromagnetic structures Ansoft HFSS (High Frequency Structural Simulator). We also aim to search and check the found optimal parameters of the helix particle. We have investigated different helices (ss and ds) of different length from 1 to 5 half-turn(s), but the following discussion

and experimental realization is based on the results for the 5 half-turn particle.

A monochromatic plane wave (3 GHz, propagating along the y-axis) excites the helix according to the model considered above. Simulations have shown that the principal surface current mode ($n = 1$) arising in the individual particle (see Figure 1) is realized at the perpendicular to the helix axis direction of the particle excitation. The current has its maximum in the center and the minimum at the ends of each half-turn. The scattered field along the z-axis is investigated in the far-field region. As the boundary conditions, we used either the perfectly matched layers or the radiation surface; they both yield adequate results. Moreover, we also used an alternative method of a full-wave integral equation solver (IE-design) which is well suited for the considered problem, because it is designed for large open problems (no boundary condition are necessary). The results for single particles show a radical difference of the ellipticities for the ss- and ds-helices (see Figure 4).

Three resonance modes can be observed: the principal resonance

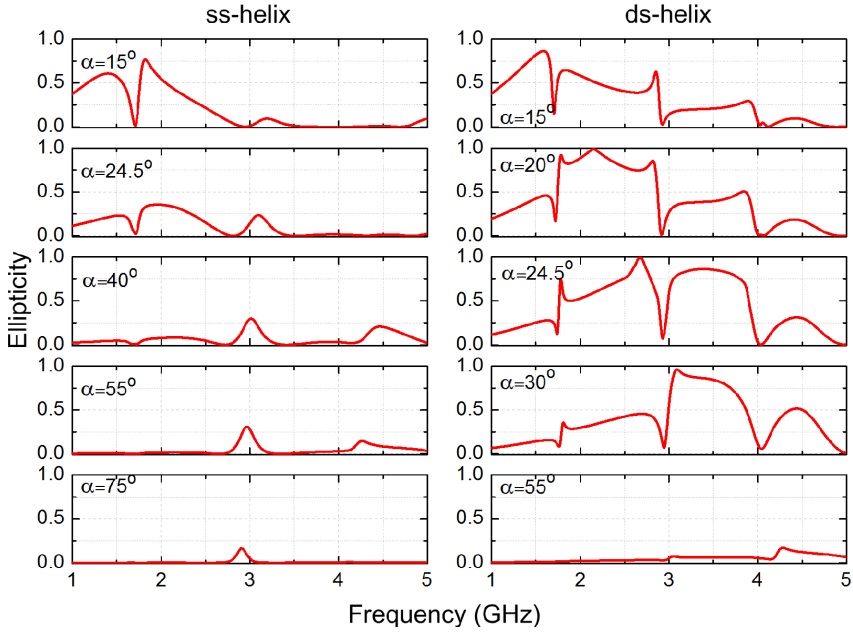

Figure 4. Polarization state evolution for individual particles (ss and ds) in a wide frequency range for various helix pitch angles (calculated in the far-field along the z-axis).

$\nu_{res} = 3\,\text{GHz}$ and less distinct $\frac{1}{2}\nu_{res}$, $\frac{3}{2}\nu_{res}$ resonances. As it was predicted by the theory, the highest value for the ellipticity is achieved at $\alpha = 55°$ for the ss-helix near the main resonance and at $\alpha = 20°$–$30°$ for the ds-helix. It is seen from these graphs that circularly polarized (or elliptical with high ellipticity) scattered waves are obtained for ds-helices (but not for the ss-helices) in a wide frequency range with the centre at the main resonance.

Total scattered intensity can be obtained theoretically from Eqs. (8) and (9) for the specified current mode. The intensity modelling results for the scattered field are shown in Figure 5. Noticeably, the intensity has strong correlation with the ellipticity resonances. The intensity maximum for the ss-helices is obtained at the main resonance frequency for the pitch angle of $\alpha = 55°$, for the ds-helices the main resonance intensity maxima are almost of the same magnitude.

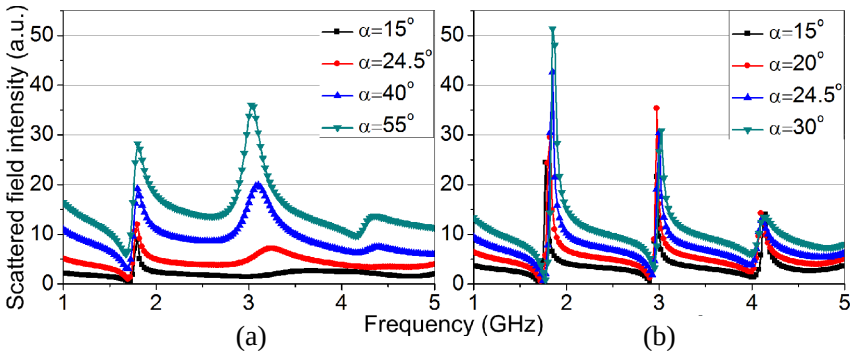

Figure 5. Scattered intensity characterization of the individual particles (ss and ds) in a wide frequency range for various helix pitch angles. (a) ss-helix. (b) ds-helix.

In Figure 6, the normalized scattered field intensity and the polarization characteristics (ellipticity) are presented for the individual ds-helix of $\alpha = 30°$ at 3.05 GHz in the yz- (perpendicular to the helix axis) and xz-planes. Here we see a pure circular polarization radiation along the z-axis with predominant intensity scattering in this direction too. The type of circular polarization was identified as left-handed (LHCP), for this polarization the curved trajectory of the E-vector of the wave (in space) is a left-handed helix. For the x- and y-axes, the ellipticity takes its minimum value close to 0.1 and, therefore, can be considered as linearly polarized. In contrast to the ds-helix, some complex distribution of total intensity was observed for the ss-helix (not shown), moreover, a steady circular polarization scattering flux was not observed.

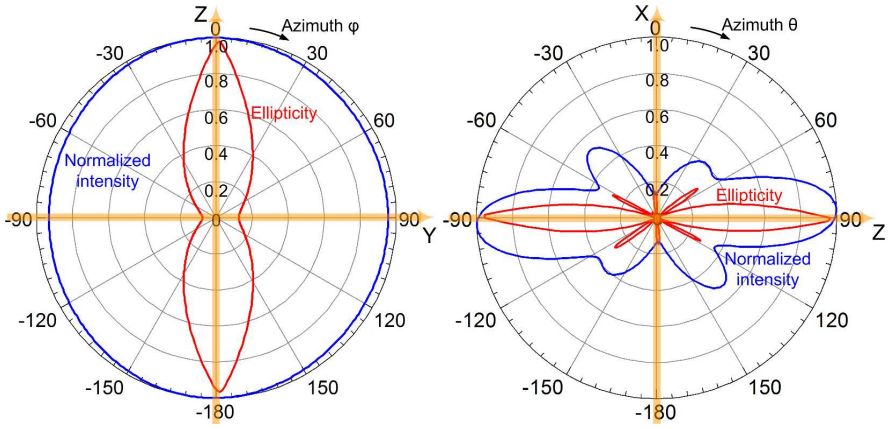

Figure 6. Scattered field and ellipticity characterization in the yz-, xz-planes for the individual ds-helix having $\alpha = 30°$ at 3.05 GHz.

Thus, strong spatial intensity re-distribution and polarization conversion are observed. The scattered intensity is almost completely concentrated in the yz-plane (perpendicular to the helix axis plane) for an individual particle. However, the total spatial intensity distribution for arrays of helices is anisotropic in the yz-plane due to mutual coupling between the helices. Moreover, these collective interactions between the helices in the array can lead to the main resonance shifting. However, the helical array investigation is out of the scope of this paper.

The results can be utilized for realization of a helical array metamaterial which has demonstrated the negative refraction phenomenon [9, 26–28]. Well known split ring resonators and fishnet structures provide negative refraction index due to an overlapping electric and magnetic resonances to achieve both negative ε and μ. As it can be seen from Eq. (2), a chiral media provide an additional parameter — the chirality parameter — for manipulating the negative index of a circularly polarized radiation [29]. Thus, in a strong birefringent media, negative refraction can be achieved without both negative ε and μ.

A disadvantage of a standard birefringent quarter wave plate is well known: it can operate only at a fixed wavelength. Design of an achromatic quarter-wave plate requires a complex combination of several retarders combined into one well adjusted device (e.g., Ref. [30]). This device can cover a wide range from 0.25 to 1.75 THz. Another example of broadband operation was demonstrated recently in Ref. [31]. The eye of a stomatopod crustacean operates as an

achromatic quarter wave retarder in the visible wavelength region due to its internal non-typical composition. Helix-shaped arrays can realize achromatic operation regime due to multiple resonance behaviour. In Ref. [12], it was reported a more than one octave operation waveband. Our late study of helix-shaped arrays in THz region demonstrated the realizability of increasing the waveband up to 1.5 octaves.

5. CONCLUSION

In this article, we have created and developed in detail the discrete dipole re-radiation model describing an individual helix intensity-polarization behavior and can be applied (to some extent) for describing a bianisotropic media composed of helical inclusions. Based on this model, we have predicted circularly polarized scattering phenomenon realized for the perpendicular to the ds-helix axis direction. Detailed analysis of helix parameters has revealed the optimal parameters of the ds-helical particle for realization of the phenomenon. The most crucial parameter is the helix pitch angle, which is optimal in the range of 20°–30° for the ds-helix.

Using computer simulations, we have demonstrated that most intensity, scattered by the ds-helix (or by the one-layer array composed of them), has unidirectional directivity and is circularly (or elliptically) polarized at the main resonance. This contrasts strongly with the directivity and the polarization type of the field scattered by the ss-helices of the same shape. Computer modeling and experimental study have confirmed the theoretically predicted model of the radiation based linear-to-circular polarization transformer.

From analysis of Figures 4 and 5 one can say about broadband operation of the ds-particle. The result of this work can be generalized to other frequency regimes such as THz and even the infrared regimes and, therefore, this work is also related to optics.

ACKNOWLEDGMENT

Financial support from The Ministry of Education, Culture, Sports, Science and Technology of Japan, Ministry of Education of Belarus, Shizuoka University and Gomel State University is acknowledged. We thank Prof. S. Tretyakov, Dr. S. Khakhomov, V. Asadchy and I. Fanyaev for helpful discussions and simulation support.

REFERENCES

1. Lindell, I. V., A. H. Sihvola, and J. Kurkijarvi, "Karl F. Lindman: The last Hertzian, and a harbinger of electromagnetic chirality," *IEEE Antennas and Propagation Magazine*, Vol. 34, No. 3, 24–30, 1992.
2. Guerin, F., P. Banneller, and M. Labeyrie, "Scattering of electromagnetic waves by helices and application to the modelling of chiral composites. I: Simple effective-medium theories," *Journal of Physics D: Applied Physics*, Vol. 28, 623, 1995.
3. Roy, J. E. and L. Shafai, "Reciprocal circular-polarization-selective surface," *IEEE Antennas and Propagation Magazine*, Vol. 38, No. 6, 18–33, 1996.
4. Hodgkinson, I. J., Q. Hong, K. E. Thorn, A. Lakhtakia, and M. W. Mccall, "Spacerless circular-polarization spectral-hole filters using chiral sculptured thin films: Theory and experiment," *Optics Communications*, Vol. 184, 57–66, 2000.
5. Yang, Z. Y., M. Zhao, P. X. Lu, and Y. F. Lu, "Ultrabroadband optical circular polarizers consisting of double-helical nanowire structures," *Optics Letters*, Vol. 35, No. 15, 2588–2590, 2010.
6. Chremmos, I., "Analytical computation of the electro-magnetic field produced by an optical fiber helix," *Progress In Electromagnetics Research B*, Vol. 16, 189–207, 2009.
7. Hady, L. K. and A. A. Kishk, "Electromagnetic scattering from conducting circular cylinder coated by metamaterials and loaded with helical strips under oblique incidence," *Progress In Electromagnetics Research B*, Vol. 3, 189–206, 2008.
8. Xiong, X., X.-C. Chen, M. Wang, R.-W. Peng, D.-J. Shu, and C. Sun, "Optically nonactive assorted helix array with interchangeable magnetic/electric resonance," *Applied Physics Letters*, Vol. 98, No. 7, 071901, 2011.
9. Semchenko, I. V., S. A. Khakhomov, and S. A. Tretyakov, "Chiral metamaterial with unit negative refraction index," *The European Physical Journal Applied Physics*, Vol. 46, No. 3, 32607, 2009.
10. Balmakov, A. P., I. V. Semchenko, S. A. Khakhomov, and M. Nagatsu, "Microwave circular polarizer based on bifilar helical particles," *Problems of Physics, Mathematics and Technics*, Vol. 1, No. 14, 7–12, 2013.
11. Guven, K., E. Saenz, R. Gonzalo, E. Ozbay, and S. Tretyakov, "Metamaterial-based cloaking with sparse distribution of spiral resonators," *Radio Science*, Vol. 7711, No. 1, 771111–771114, 2010.

12. Wu, C., H. Li, X. Yu, F. Li, H. Chen, and C. Chan, "Metallic helix array as a broadband wave plate," *Physical Review Letters*, Vol. 107, No. 17, 1–5, 2011.
13. Semchenko, I. V., S. A. Khakhomov, E. V. Naumova, V. Y. Prinz, S. V. Golod, and V. V. Kubarev, "Study of the properties of artificial anisotropic structures with high chirality," *Crystallography Reports*, Vol. 56, No. 3, 366–373, 2011.
14. Seet, K. K., V. Mizeikis, S. Juodkazis, and H. Misawa, "Three-dimensional horizontal circular spiral photonic crystals with stop gaps below 1 µm," *Applied Physics Letters*, Vol. 88, No. 22, 221101, 2006.
15. Volakis, J. L., *Antenna Engineering Handbook*, 4th Edition, 1754, McGraw-Hill Co., 2007.
16. Serdyukov, A., I. Semchenko, S. Tretyakov, and A. Sihvola, *Electromagnetics of Bi-anisotropic Materials: Theory and Applications,* 337, Gordon and Breach, New York, 2001.
17. Jaggard, D. L., A. R. Mickelson, and C. H. Papas, "On electromagnetic waves in chiral media," *Applied Physics*, Vol. 18, No. 2, 211–216, 1979.
18. Landau, L. D. and E. M. Lifshitz, *The Classical Theory of Fields*, 4th Edition, 428, Butterworth-Heinemann, 1980.
19. Yavorsky, B. M., A. A. Detlaf, and N. Weinstein, *Handbook of Physics*, 4th Edition, 965, Central Books Ltd., 1973.
20. Balanis, C. A., *Antenna Theory*, 2nd Edition, 960, John Wiley and Sons, Inc., 1996.
21. Semchenko, I. V., S. A. Khakhomov, and A. P. Balmakov, "Polarization selectivity of electromagnetic radiation of deoxyribonucleic acid," *Journal of Communications Technology and Electronics*, Vol. 52, No. 9, 996–1001, 2007.
22. Semchenko, I., S. Khakhomov, and A. Balmakov, "Polarization selectivity of interaction of DNA molecules with X-ray radiation," *Biophysics*, Vol. 55, No. 2, 194–198, 2010.
23. Semchenko, I. V., S. A. Khakhomov, and A. L. Samofalov, "Transformation of the polarization of electromagnetic waves by helical radiators," *Journal of Communications Technology and Electronics*, Vol. 52, No. 8, 850–855, 2007.
24. Watson, J. D. and F. H. C. Crick, "A structure for deoxyribose nucleic acid," *Nature*, Vol. 171, No. 4356, 737–738, 1953.
25. Mandelkern, M., J. G. Elias, D. Eden, and D. M. Crothers, "The dimensions of DNA in solution," *Journal of Molecular Biology*, Vol. 152, No. 1, 153–161, 1981.

26. Wu, C., H. Li, Z. Wei, X. Yu, and C. T. Chan, "Theory and experimental realization of negative refraction in a metallic helix array," *Physical Review Letters*, Vol. 105, 247401, 2010.
27. Cheng, Q. and T. Cui, "Negative refractions in uniaxially anisotropic chiral media," *Physical Review B*, Vol. 73, No. 11, 1–4, 2006.
28. Balmakou, A., I. Semchenko, and M. Nagatsu, "Realization of negative refraction in a bifilar prism-type array metamaterial," *Applied Physics Express*, Vol. 6, 072601, 2013.
29. Tretyakov, S., I. Nefedov, A. Sihvola, S. Maslovski, and C. Simovski, "Waves and energy in chiral nihility," *Journal of Electromagnetic Waves and Applications*, Vol. 17, No. 5, 695–706, 2003.
30. Masson, J. and G. Gallot, "Terahertz achromatic quarter-wave plate," *Optics Letters*, Vol. 31, No. 2, 265–267, 2006.
31. Roberts, N. W., T.-H. Chiou, N. J. Marshall, and T. W. Cronin, "A biological quarter-wave retarder with excellent achromaticity in the visible wavelength region," *Nature Photonics*, Vol. 189, 1038, 2009.